




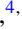



Coherent treatment of transfer-excitation processes in swift ion-atom collisions

A. Laoutaris ^{1,2}, S. Nanos ^{3,2}, I. Madesis ^{1,2}, S. Passalidis ⁴, E. P. Benis ³, A. Dubois ^{4,*} and T. J. M. Zouros ^{1,†}

¹*Department of Physics, University of Crete, GR-70013 Heraklion, Greece*

²*Tandem Accelerator Laboratory, Institute of Nuclear and Particle Physics, NCSR “Demokritos”, GR-15310 Ag. Paraskevi, Greece*

³*Department of Physics, University of Ioannina, GR-45110 Ioannina, Greece*

⁴*Sorbonne Université, CNRS, Laboratoire de Chimie Physique-Matière et Rayonnement, F-75005 Paris, France*



(Received 21 July 2021; revised 16 February 2022; accepted 2 August 2022; published 17 August 2022)

For more than 40 years since the first ion-atom collision investigations of the two-electron process of electron transfer with excitation and its resonant and nonresonant features, a satisfactory quantum mechanical treatment has been lacking. We present now such a comprehensive transfer excitation treatment using a three-electron atomic orbital close-coupling approach within a full configuration interaction formalism, exemplified by $C^{4+}(1s^2) + He$ collisions at 0.5–18 MeV impact energies. The calculated cross sections for the production of $C^{3+}(1s2p^2\ ^2D)$, which shows the strongest resonance signature among the KLL Auger transitions, are found to be in excellent agreement with zero-degree Auger projectile spectroscopy measurements covering the maximum of the resonance peak and its high energy wing. At the lower energies, the theoretical results show a second maximum which is interpreted through a nonresonant one-step transfer excitation mechanism, never considered to date. The present, fully coherent, many-body treatment provides an important advance in the modeling and understanding of multielectronic processes in quantum systems under strong and ultrafast perturbations.

DOI: [10.1103/PhysRevA.106.022810](https://doi.org/10.1103/PhysRevA.106.022810)

I. INTRODUCTION

The understanding and modeling of the dynamics of many-body quantum systems under intense, ultrafast perturbations is nowadays a great challenge in physics and chemistry, for atoms and molecules in the gas phase or in condensed matter [1–3]. Energetic (MeV) collisions of few-electron ions with atomic targets provide ideal laboratories to address such challenges. Indeed, the interaction time in such collisions is much smaller than 1 fs, while the interplay between the electron-nucleus (e-n) and electron-electron (e-e) interactions, as well as electron exchange effects, remains complex. Though these can now be very efficiently taken into account in atomic, molecular, or condensed matter systems in the ground state or near equilibrium, as in quantum chemistry (e.g., see [4]), the theory and modeling have yet to reach a similar level of sophistication for dynamical quantum systems such as ion-atom/molecule collisions. Even so, such few-electron collision systems are still sufficiently simple to allow for an understanding based on the individual particle interactions [5]. In particular, special interests and challenges exist when considering the dynamic effect of the interactions between two electrons located on different centers (also known as two-center e-e interactions). This is especially true for electron transfer with excitation (TE) occurring in ion-atom collisions [6,7] or interatomic Coulombic decay (ICD) in weakly bound systems [8].

A fully coherent treatment, as well as a direct comparison with experiment, as proposed for example in ICD systems

[10], has in general been lacking in the description of multielectronic processes for swift ion-atom collisions. In this work we present such a coherent treatment with experimental support for the process of TE occurring in MeV ion-atom collisions. TE is a two-electron process involving the excitation of a projectile electron with the simultaneous transfer of a target electron resulting in a doubly excited projectile state. Interest in TE, and particularly its high energy resonant character, has been partly generated by its close relation to the electron-ion collision process of dielectronic capture, a process where a free electron may be captured by an ion, with important applications to plasma cooling (e.g., see [11] and references therein). In asymmetric collisions of heavy projectiles with light targets two distinct peaks are typically observed in the TE cross sections as a function of impact energy [7,12]: A high-energy peak designated as resonant transfer excitation (RTE) [6], and a low-energy peak designated as nonresonant transfer excitation (NTE) [7,13,14]. Both RTE and NTE mechanisms are shown schematically in Fig. 1. The relative importance of these two distinct peak structures in the TE cross section has been evidenced experimentally utilizing a variety of different techniques (see reviews [9,15] and references therein), primarily through their dependence on impact energy, projectile charge, and target species. In particular, state-selective TE measurements have been realized, especially for the lowest atomic number Z_p projectile ions, by high resolution Auger projectile spectroscopy [16–25] and have provided the most stringent tests of theory.

Two different models have been developed to elucidate the impact energy dependence of the TE cross sections. The RTE contribution has been described to first order by a one-step mechanism mediated by the two-center e-e interaction (TCee) (see Fig. 1 top). It has been modeled through the impulse

*alain.dubois@sorbonne-universite.fr

†tzouros@physics.uoc.gr

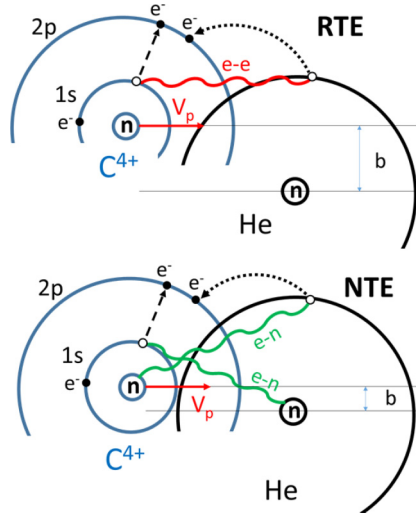


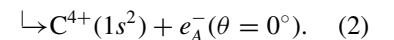
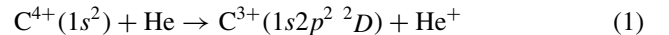
FIG. 1. Schematic of known TE mechanisms leading to the production of the doubly excited projectile $C^{3+}(1s2p^2\ ^2D)$ level in collisions of $C^{4+}(1s^2) + He$, of interest here. Indicated in red is the two-center electron-electron ($e-e$) interaction (TCee), while in green the electron-nucleus ($e-n$) interaction. The $1s \rightarrow 2p$ projectile excitation is indicated by a straight dashed arrow, while the transfer of a target electron to the projectile $2p$ by a curved dotted arrow. Also indicated are the projectile velocity V_p in red and the impact parameter b . (Top) Resonant transfer excitation (RTE), mediated by the TCee interaction, in which both excitation and transfer occur simultaneously in the *same single step* and are therefore correlated, and (bottom) nonresonant transfer excitation (NTE), mediated by two separate ($e-n$) interactions taking place in a *sequence* of uncorrelated events. Figure adapted from Ref. [9].

approximation (IA), as a quasifree resonant electron scattering analogous to the inverse Auger process [17,18,26,27]. However, the IA, even though fairly successful in describing the relative collisional energy dependence of RTE, is not an ion-atom collision theory, but is based on an electron impact theory adjusted for the initial energy distribution of the electron according to the momentum distribution (Compton profile) of the target electron carried into the collision. On the other hand, the NTE contributions have been interpreted by a sequence of uncorrelated excitation and transfer events, each independently driven by separate $e-n$ interactions [28,29] (see Fig. 1 bottom). Both TE mechanisms can be expected to occur in the same ion-atom collision contributing *coherently* to the production of the same final (doubly excited) projectile state. To date, calculated cross sections for these different TE mechanisms have only been computed separately in independent treatments. Thus, their contributions to the total TE cross sections could only be added incoherently, allowing at most for interesting speculations about possible RTE-NTE interferences [5,16,25,28,30–32]. Such *ad hoc* treatments cannot be considered satisfactory and the development of a coherent approach to properly describe transfer excitation within an ion-atom collision framework has been long awaited.

Up to now, the theoretical description of TE within coherent approaches has proven problematic, essentially due to the difficulty of including several electrons and both $e-e$ and $e-n$ interactions within the same dynamical treatment

[5,33]. Only two such dynamical treatments have appeared so far in which the signatures of RTE and NTE have been sought, both involving two-electron collision systems: (i) the two-electron atomic orbital close-coupling (CC) treatment [28], and (ii) the continuous distorted wave four-body (CDW-4B) approach [34–36]. The CC calculations were carried out for the benchmark near symmetric $He^+(1s) + H(1s)$ system. Stemming from a minimal CC basis set, the cross sections for the dominant $He(2p^2\ ^1D)$ RTE resonance were found to be much larger than measurements for an H_2 target (see [37] and Fig. 6 in [9]). Nevertheless, this approach showed the way for such exact nonperturbative TE treatments, while introducing a refined model to assess the RTE contributions. The CDW-4B was applied mainly to highly asymmetric systems (e.g., $S^{15+} + H$ [34] and references therein). The computed cross sections were compared at the RTE peak to low resolution x-ray measurements making an accurate quantitative interpretation difficult. On the other hand, the NTE peak was too low in collision energy to be described by CDW-4B. This approach was also applied to the $He^+ + He$ [16,35] and $He^+(1s) + H$ [36] systems, but found to disagree strongly with both experiment and the previously mentioned CC results of Ref. [28]. Since then, due to the difficulties of such computations and measurements, no further attempts have been made towards a comprehensive coherent treatment.

In this work we present a nonperturbative treatment of transfer excitation occurring in 0.5–18 MeV collisions between a two-electron projectile $C^{4+}(1s^2)$, and a helium target. We focus on the production of the $C^{3+}(1s2p^2\ ^2D)$ state (for short 2D in the following), which shows the strongest RTE resonance [9,24] among the KLL Auger transitions, i.e., on the TE process of Eq. (1),



Cross sections were experimentally determined using zero-degree Auger projectile spectroscopy (ZAPS) [38] by detecting the emitted 2D Auger electrons at $\theta = 0^\circ$ with respect to the beam direction [see Eq. (2)]. Our theoretical treatment considers the dynamics of three active electrons using semi-classical close-coupling calculations (referred to as 3eAOC in the following), within a full configuration interaction approach [39]. This implementation allows for a coupled and coherent treatment of all processes such as target and projectile excitation, ionization, single electron capture, as well as TE and therefore goes well beyond the methods developed in the past.

In a recent publication [40] we have reported experimental and theoretical results, relating to single electron capture to the metastable $1s2s\ ^3S$ component of the C^{4+} ion beam, using the same experimental apparatus and theoretical approach. Thus, for pertinent details, we refer the reader to this publication.

II. EXPERIMENT

Our measurements were conducted at the National Center for Scientific Research (NCSR) “Demokritos” 5.5 MV tandem accelerator facility [41], utilizing the ZAPS setup (for

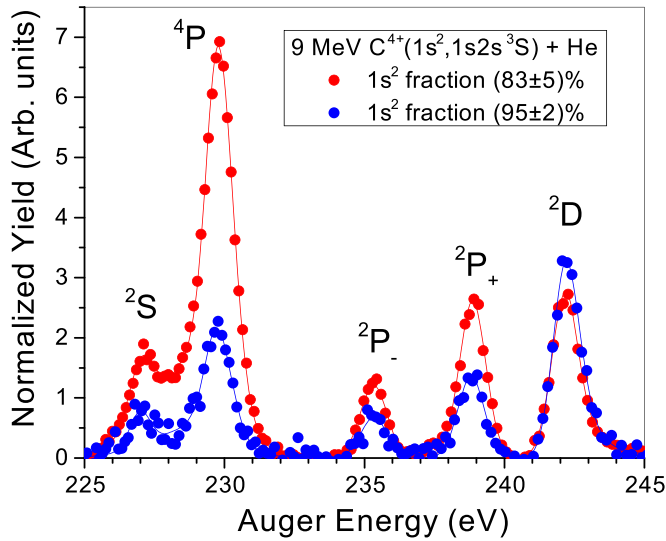


FIG. 2. Typical $C^{3+}(1s2l2l')$ Auger KLL spectra showing the $1s2s^2 2S$, $1s2s2p 4P$, $1s2s2p 2P_{\pm}$, and the $1s2p^2 2D$ lines obtained in collisions of mixed-state $C^{4+}(1s^2, 1s2s 3S)$ ion beams with helium target. The $2D$ is assumed to be *exclusively* produced from the ground state component by transfer excitation, while the $4P$ is *exclusively* produced by single electron capture to the metastable $1s2s 3S$ component. The two spectra are obtained from C^{4+} ion beams with different $1s2s 3S$ admixtures f_3 (and therefore also different ground state $1s^2$ fractions, $f_g = 1 - f_3$) controlled by varying the ion stripping conditions.

more details see [40,42]), centered around a hemispherical electron spectrograph with a preretardation lens. The absolute overall spectrograph efficiency was obtained by performing auxiliary *in situ* measurements of elastically scattered (binary encounter) electrons from bare C^{6+} ion beams, as typically done for increased accuracy in all such ZAPS measurements [38,43]. The $C^{4+}(1s^2)$ ions, with about 5%–30% admixture of $C^{4+}(1s2s 3S)$ metastable component, were accelerated to 6–18 MeV with 0.2–20 nA beam intensities on target. Due to the millisecond lifetime of the $C^{4+}(1s2s 3S)$ state [44], this beam component may also survive to the target [45] contributing, in general, to the production of the $C^{3+}(1s2l2l')$ states [46] and can thus be a considerable obstacle in measurements, where only the ground state contribution is of interest [e.g., Eq. (1)]. In the collision energy range measured here, the $2D$ is almost exclusively produced from the ground state of the ion beam. This component has been shown to be accurately determined *in situ* using our recently proposed “two-spectra measurement” technique [42,46].

In this technique, two different measurements of the same Auger KLL spectrum, but with beams prepared with *different* $1s^2$ fractional content, are utilized (a typical example is shown in Fig. 2). Such beams can be readily prepared in lower or higher amounts of ground state component by stripping the ion beam, either in the tandem accelerator terminal, or after ion charge selection and energy analysis, in a post-stripper, usually in gas or thin self-supporting foils [47–50], respectively. Then, noting further that the $1s2s2p 4P$ Auger line (see Fig. 2) due to spin considerations is *exclusively* produced from the metastable $1s2s 3S$ component [40,51], the beam

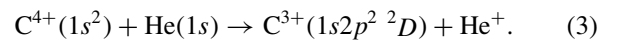
composition can be obtained [45,46,49]. Furthermore, in the case where the observed KLL Auger lines can be populated from both ground state and metastable state components, our two-measurement technique [46] can directly determine each contribution without the need to explicitly know the amount of metastable admixture, but just from the measurement of the relative intensities in the two spectra [40].

In Table I the measured $\theta = 0^\circ$ Auger single differential cross sections (SDCS), $d\sigma_A^{\text{expt}}(0^\circ)/d\Omega$ for the $2D$, and ground state fractions f_g are listed. In some cases, as marked, just a single spectrum was used whose ground state fraction was then interpolated. The stripping methods are marked as gas terminal stripping (GTS), foil terminal stripping (FTS), gas post-stripping (GPS), foil post-stripping (FPS), and their combinations. These stripping methods are explained in more detail in Ref. [45]. The listed SDCS are also displayed in Fig. 3.

III. THEORY

A. 3eAOCC calculations

The 3eAOCC calculations involve three active electrons, modeling the helium target with just one electron, in order to have the most accurate description of C^{4+} and C^{3+} electronic structures. The process then theoretically considered can be written schematically as



The calculations were performed for 0.5–18 MeV impact energies, covering the entire range of interest. We have adopted a semiclassical close-coupling (CC) approach, based on an asymptotic (atomic) description of the scattering event, as previously used for various collision systems and processes, e.g. [39,40,51,54–56] (see also [57,58] for a more detailed description). Here we just outline the main features of the method as they relate to the present calculations. The electronic dynamics is described by solving nonperturbatively the time-dependent Schrödinger equation (TDSE) for a three-electron Hamiltonian, including the Coulombic interactions between all particles. The helium target is described within a single active electron picture, using a model potential, as previously used in [40,51]. Thus, all results have been multiplied by 2 to account for the two target electrons in an independent particle approximation. The spin-orbit couplings, being small, were not taken into account. The total scattering wave function is then expanded in terms of three-electron states, which allows for an accurate description of the important $C^{3+}(1s2l2l' 2S+1L)$ TE channels. To describe the He, C^{4+} , and C^{3+} electronic states, we use the same Gaussian-type orbital (GTO) sets as in [51] from which spin-adapted products are constructed to diagonalize the isolated target and projectile Hamiltonians within a full configuration interaction (CI) formalism. The TDSE then reduces to a set of coupled differential equations for the time-dependent coefficients, which asymptotically are the probability amplitudes from which cross sections are evaluated. The calculations presented in this work include 1794 states (or 716 energy levels), referred to as full CC (FCC) in the following and represent several thousands of hours of computation. They have been tested for possible numerical issues, as well as by changing the GTO sets and the number of states included in the basis sets. These

TABLE I. Theoretical and experimental results for the $1s2p^2\ ^2D$ state produced in collisions of $C^{4+}(1s^2)$ with He [see Eq. (1)] at a projectile velocity V_p and energy E_p , respectively. Listed are the full 3eAOCC (FCC) partial cross sections $\sigma(2, |M_L|)$ for $M_L = 0, \pm 1, \pm 2$, already multiplied by 2 to account for the two electrons on the helium target, the total production cross section σ_{tot} , and the theoretical 0° Auger SDCS, $d\sigma_A(0^\circ)/d\Omega$. Also listed are the ion beam stripping combinations used in the measurements (see Sec. II for explanations) with the first/second measurement indicated by the separator /, in the case of two-spectra measurements. Finally, the ground state fraction f_g , the measured 0° Auger electron normalized yields $dY_A(0^\circ)/d\Omega$ [49], and the experimentally determined 0° Auger SDCS, $d\sigma_A^{\text{expt}}(0^\circ)/d\Omega$ [46] are also indicated. Both experimental and theoretical SDCS are shown in Fig. 3. Experimental uncertainties in the SDCS include both the statistical error and the uncertainty in the fraction f_g , when single spectrum measurements are involved. In the case of two-spectra measurements only statistical uncertainties are involved [46]. Entries indicated by – means no result was acquired, while an empty (blank) entry means this entry is the same as in the previous line and column. The notation $4.31(-1)$ stands for 4.31×10^{-1} .

V_p (a.u.)	E_p (MeV)	Theory (FCC)					Experiment					
		$\sigma(2, 0)$	$\sigma(2, 1)$	$\sigma(2, 2)$	σ_{tot}^a	$\frac{d\sigma_A}{d\Omega}(0^\circ)^b$	Stripping method	$f_g^{[1]c}$ (%)	$f_g^{[2]c}$ (%)	$\frac{dY_A^{[1]}}{d\Omega}(0^\circ)$	$\frac{dY_A^{[2]}}{d\Omega}(0^\circ)$	$\frac{d\sigma_A^{\text{expt}}}{d\Omega}(0^\circ)^d$
		(cm^2) $(\times 10^{-21})$									(cm^2/sr) $(\times 10^{-21})$	
1.291	0.50	6.58(-1)	1.84(-1)	1.69(-2)	1.06	2.62(-1)	–	–	–	–	–	–
1.826	1.00	1.47(1)	4.90	5.57(-1)	2.56(1)	5.84	–	–	–	–	–	–
2.582	2.00	3.46(1)	1.48(1)	8.61(-1)	6.59(1)	1.38(1)	–	–	–	–	–	–
3.162	3.00	3.26(1)	1.36(1)	1.07	6.18(1)	1.30(1)	–	–	–	–	–	–
3.652	4.00	3.48(1)	1.03(1)	7.56(-1)	5.69(1)	1.38(1)	–	–	–	–	–	–
4.082	5.00	4.54(1)	8.05	4.31(-1)	6.24(1)	1.81(1)	–	–	–	–	–	–
4.472	6.00	5.06(1)	6.51	2.25(-1)	6.40(1)	2.01(1)	GTS-FPS ^e	–	85.5 ± 5.1	–	18.9 ± 1.3	22.2 ± 2.1
							GTS-GPS/GTS ^g	83.6 ± 3.1	93.3 ± 1.3	20.5 ± 0.2	22.9 ± 0.5	24.5 ± 0.8
4.830	7.00	4.33(1)	4.93	1.18(-1)	5.34(1)	1.72(1)	GTS-FPS ^e	–	85.5 ± 5.1	–	16.2 ± 1.1	19.0 ± 1.7
5.164	8.00	3.08(1)	3.50	6.70(-2)	3.79(1)	1.23(1)	GTS-FPS ^e	–	85.5 ± 6.2	–	10.4 ± 0.7	12.2 ± 1.2
5.477	9.00	1.98(1)	2.37	4.23(-2)	2.46(1)	7.88	GTS-FPS ^e	–	85.5 ± 5.1	–	4.58 ± 0.19	5.37 ± 0.39
							GTS-GPS/GTS ^g	82.5 ± 5.3	94.5 ± 1.7	3.95 ± 0.06	4.53 ± 0.20	4.79 ± 0.29
5.657	9.60	–	–	–	–	–	GTS-FPS ^e	–	85.5 ± 5.1	–	4.37 ± 0.46	5.12 ± 0.62
5.774	10.00	1.22(1)	1.56	2.87(-2)	1.53(1)	4.85	avg ^f	–	89.0 ± 5.1	–	2.88 ± 0.37	3.24 ± 0.45
6.325	12.00	4.62	6.60(-1)	1.47(-2)	5.97	1.84	GTS ^e avg ^f	–	84.6 ± 5.1	–	1.04 ± 0.01	1.13 ± 0.21
							FTS/GTS ^g	79.3 ± 4.9	96.5 ± 0.9	0.854 ± 0.017	1.04 ± 0.05	1.08 ± 0.06
6.709	13.50	–	–	–	–	–	GTS ^e	–	92.7 ± 13.9	–	0.335 ± 0.030	0.363 ± 0.063
7.071	15.00	1.26	1.87(-1)	6.24(-3)	1.64	5.00(-1)	GTS ^e avg ^f	–	83.8 ± 12.6	–	0.255 ± 0.061	0.305 ± 0.086
							FTS/GTS ^g	86.3 ± 8.4	93.9 ± 3.8	0.355 ± 0.010	0.386 ± 0.019	0.412 ± 0.036
7.746	18.00	4.12(-1)	5.99(-2)	3.18(-3)	5.39(-1)	1.64(-1)	FTS ^e	–	71.0 ± 4.3	–	0.0584 ± 0.024	0.083 ± 0.034

^aFor the 2D state σ_{tot} is given by Eq. (7).

^bTheoretical 0° Auger SDCS for the 2D state, $d\sigma_A(0^\circ)/d\Omega$, determined from the partial cross sections $\sigma(2, M_L)$ according to Eq. (8).

^cThe ground state fraction $f_g^{[i]}$ in measurement i ($i = 1, 2$) is computed from the experimentally determined $1s2s\ ^3S$ metastable state fraction $f_{3S}^{[i]}$ [45,46] as $f_g^{[i]} = 1 - f_{3S}^{[i]}$.

^dExperimental 0° Auger SDCS for the 2D state, $d\sigma_A^{\text{expt}}(0^\circ)/d\Omega = [dY_A^{[i]}(0^\circ)/d\Omega]/f_g^{[i]}$.

^eResults obtained using single Auger KLL spectrum measurements [52] with an f_g value interpolated from similar nearest energy two-spectra measurements.

^fAn average (avg) value was computed when more than one measurements were made having similar values of ground state fraction f_g at the same collision energy.

^gResults [51,53] obtained using the two-spectra measurement technique [46].

tests allow us to place a conservative confidence interval of about 15% on all presented cross sections. In Table I the calculated total σ_{tot} and partial cross sections $\sigma(L, |M_L|)$ for the 2D are listed. They are displayed in Fig. 5 (top).

B. The $1s2p^2\ ^2D$ Auger SDCS and angular distributions

The 2D SDCS were then computed using the Auger angular distribution (Legendre polynomial expansion) formula [59]:

$$\frac{d\sigma_A}{d\Omega}(\theta) = \bar{\xi} \frac{\sigma_{\text{tot}}}{4\pi} [1 + A_2 P_2(\cos \theta) + A_4 P_4(\cos \theta)], \quad (4)$$

where $\bar{\xi} = 0.9989$ is the mean 2D Auger yield [60] and the anisotropy coefficients A_2, A_4 are functions of the 2D partial M_L -resolved cross sections. In LS coupling these coefficients depend only on L and $|M_L|$ [59] and are given by

$$A_2 = \left(\frac{10}{7}\right) \frac{\sigma(2, 0) + \sigma(2, 1) - 2\sigma(2, 2)}{\sigma_{\text{tot}}}, \quad (5)$$

$$A_4 = \left(\frac{6}{7}\right) \frac{3\sigma(2, 0) - 4\sigma(2, 1) + \sigma(2, 2)}{\sigma_{\text{tot}}}. \quad (6)$$

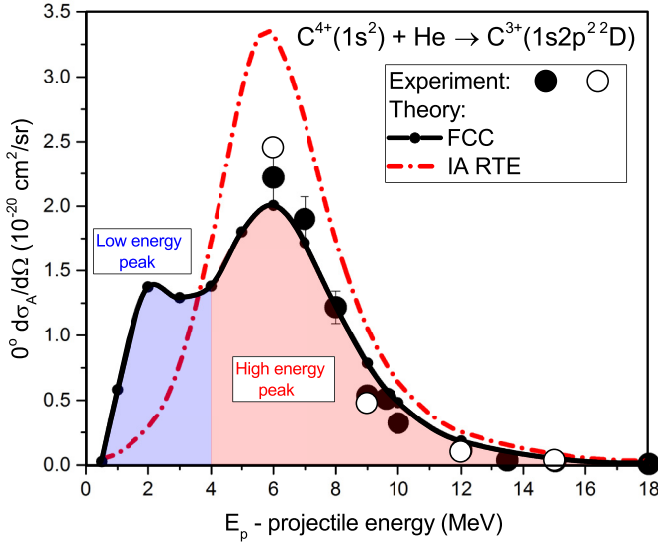


FIG. 3. Projectile energy dependence of absolute 0° Auger SDCS, $d\sigma_A/d\Omega$ [Eq. (8)], for the production of 2D states by TE [Eq. (1)]. Experiment (large circles, see Table I): Filled (single-spectra measurements), open (two-spectra measurements). Error bars shown only when larger than symbol. Below 6 MeV, measurements were not possible due to beam current limitations. Theory: Full $3eAOCC$ TE (FCC, small circles joined by black interpolation line). IA RTE [red dash-dotted line, see Eq. (9)].

The total 2D production cross section σ_{tot} is

$$\sigma_{\text{tot}} = \sum_{M_L=-L}^L \sigma(L, |M_L|) = \sigma(2, 0) + 2\sigma(2, 1) + 2\sigma(2, 2), \quad (7)$$

where, due to the axial symmetry around the beam direction, we also have $\sigma(L, M_L) = \sigma(L, -M_L)$. For $\theta = 0^\circ$ in Eq. (4), with $P_k(\cos 0^\circ) = 1$ for k even, we then directly have

$$\frac{d\sigma_A}{d\Omega}(\theta = 0^\circ) = \bar{\xi} \frac{5\sigma(2, 0)}{4\pi}, \quad (8)$$

showing that at this observation angle the SDCS depend only on the $M_L = 0$ component of the partial cross section $\sigma(2, 0)$. Further corrections due to fine-structure interaction during the time interval between production and Auger decay, i.e., the so called dealignment factors D_2 and D_4 [59], differ very little from 1 for the $C^{3+}(1s2p^2 {}^2D)$ state [61], with this correction well within the experimental uncertainty and therefore considered negligible.

In Table I the $\theta = 0^\circ$ Auger SDCS, $d\sigma_A(0^\circ)/d\Omega$, calculated according to Eq. (8) for the 2D , are also listed. They are displayed in Fig. 3.

IV. RESULTS AND DISCUSSION

The experimentally extracted $\theta = 0^\circ$ Auger SDCS, $d\sigma_A^{\text{expt}}(0^\circ)/d\Omega$, are shown in Fig. 3 as a function of the impact energy E_p , together with our theoretical FCC results. Also included is the RTE impulse approximation (IA RTE) [19], seen to be about 30% larger than experiment, a known deficiency for low- Z_p ions [9]. Our FCC results (thick black line) show

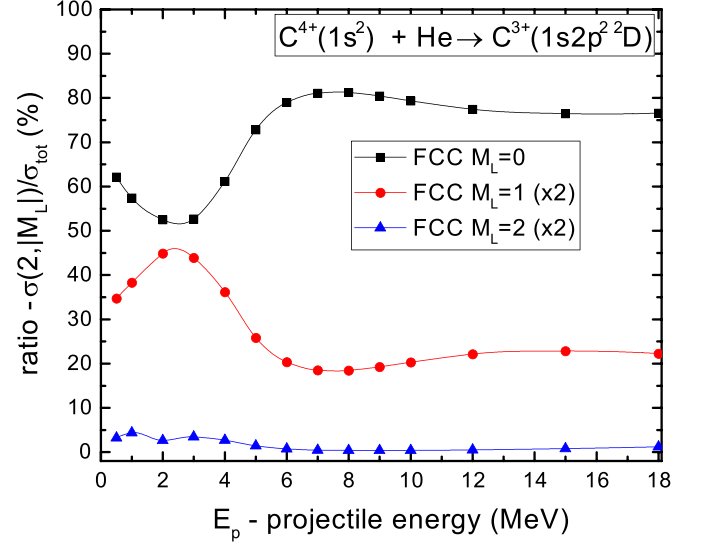


FIG. 4. FCC results of ratios of partial to total cross sections $\sigma(L=2, |M_L|)/\sigma_{\text{tot}}$ as a function of projectile energy. A strong $M_L = 0$ contribution is observed for collision energies above 6 MeV where the high-energy peak lies.

two distinct peaks. The side of the peak above 6 MeV is seen to be in excellent agreement with our ZAPS measurements, not only in the energy dependence, but also in the absolute scale. The low-energy peak located around 2 MeV could not be recorded experimentally since the C^{4+} beam intensity was too low for reliable ZAPS measurements in this difficult to access 0.5–4 MeV range.

Additionally, in Fig. 4 the fractional contribution of each M_L component to the total production for the 2D state is shown. The high energy peak associated with RTE is seen to be dominated by $M_L = 0$ contributions, as expected from the impulse approximation inverse Auger description of this process given by [9,62]

$$\frac{d\sigma_{\text{RTE}}^{\text{IA}}}{d\Omega'}(\theta) = \bar{\xi} \sigma_{\text{RTE}}^{\text{IA}} Y_{L0}^2(\theta, \phi), \quad (9)$$

where Y_{L0} is the $M_L = 0$ component of the spherical harmonic $Y_{LM_L}(\theta, \phi)$ and $\sigma_{\text{RTE}}^{\text{IA}}$ is the total IA RTE cross section [9,22]. The M_L dependence is seen to then change quite drastically between 2 and 4 MeV, where the $M_L = 1$ contributions become of about equal importance signifying the possible onset of a different mechanism. Finally, the $M_L = 2$ component is seen to be much smaller and quite constant over the entire collision energy range.

A. Two-level model calculations: Suppressing the two-step mechanism

To get further insight into the electronic dynamics, we also performed two-level calculations to model the production of the $C^{3+}(1s2p^2 {}^2D)$ and $C^{3+}(1s2p^2 {}^2P)$ states. The comparison of these identically configured states [63] offers indeed additional interesting insights into the mechanisms of their production [28].

In contrast to the (716-level) FCC results, which include both 2D and 2P levels, these two-level CC calculations used

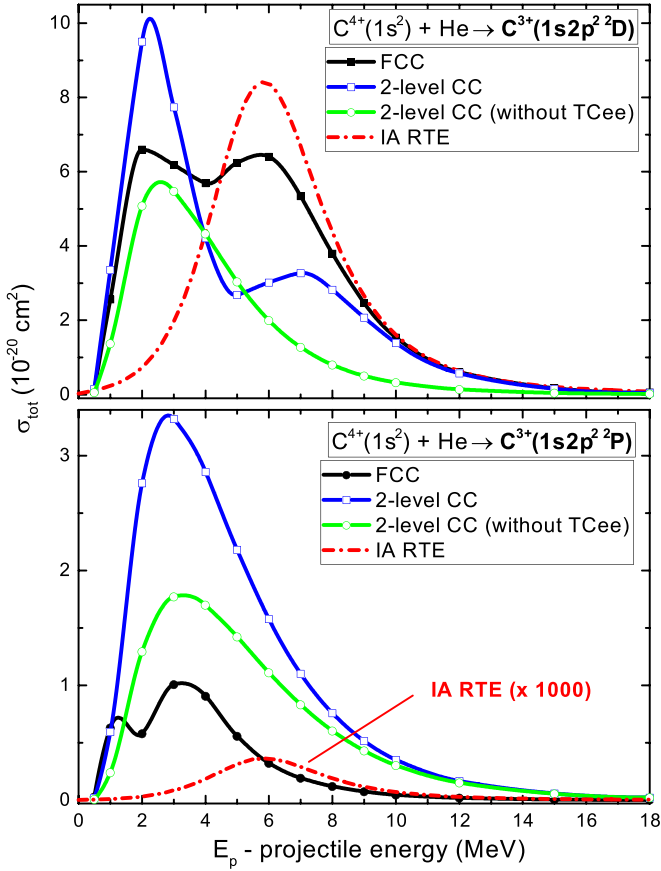


FIG. 5. Projectile energy dependence of theoretical total cross sections σ_{tot} for the production of the similarly configured $1s2p^2 \ ^2D$ (top) and $1s2p^2 \ ^2P$ (bottom) states. Black lines with filled squares: Full close-coupling (FCC) calculations (used in the SDCS shown in Fig. 3). Blue lines with open squares: Two-level calculations. Green lines with open circles: Two-level CC without TCee. Red dashed dot lines: IA RTE cross sections $\sigma_{\text{RTE}}^{\text{IA}}$, also shown for both states.

a restricted basis set, including only the initial level, i.e., the target and projectile ground states, and either one of the final 2D or 2P levels, with their five or three M_L magnetic states, respectively. Without including any single excitation and single capture states, this simplified model blocks these specific channels and therefore deliberately suppresses any two-step mechanisms involving excitation and capture such as NTE [28]. As in the FCC calculations, they include all interactions and couplings between the states. In addition, we developed a second two-level model in which, for the same restricted basis set, the coupled equations are similarly solved, but without the two-center e-e coupling matrix elements [referred to from here on as two-level CC (without TCee)], thus further blocking also processes mediated by TCee such as RTE. In the following we present our theoretical results for the 2D and 2P states. Their total production cross sections stemming from these different calculations are presented in Fig. 5, while the related reduced probabilities $bP(b)$ in Figs. 6 and 7. The latter offer additional information on the nature of the production mechanisms, related to head-on (hard) or distant (soft) collisions.

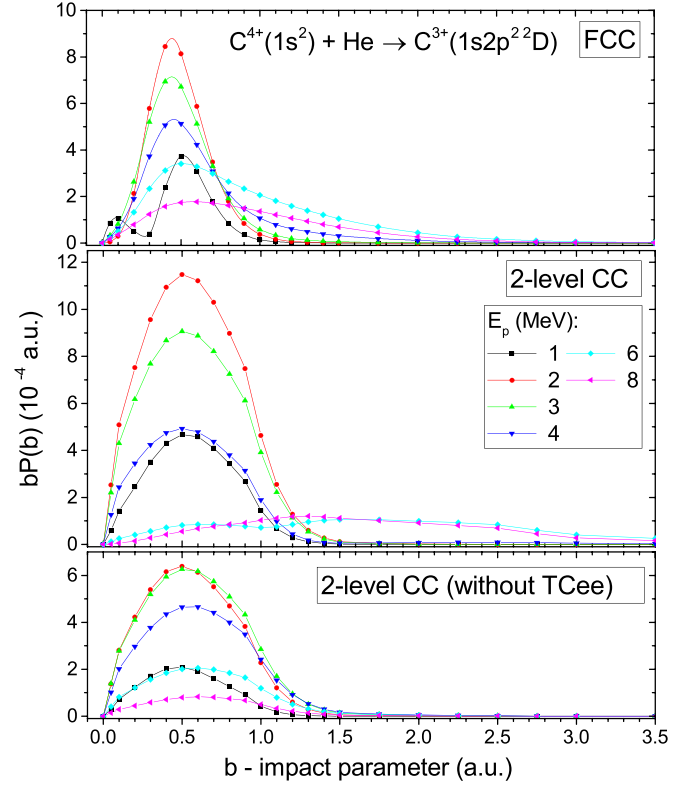


FIG. 6. Impact parameter-weighted TE probabilities $bP(b)$ (multiplied by 2 to account for the two target electrons) as a function of impact parameter b for the $1s2p^2 \ ^2D$ state at selected projectile energies $E_p = 1, 2, 3, 4, 6,$ and 8 MeV. The three panels from top to bottom correspond to our three different calculations (see text).

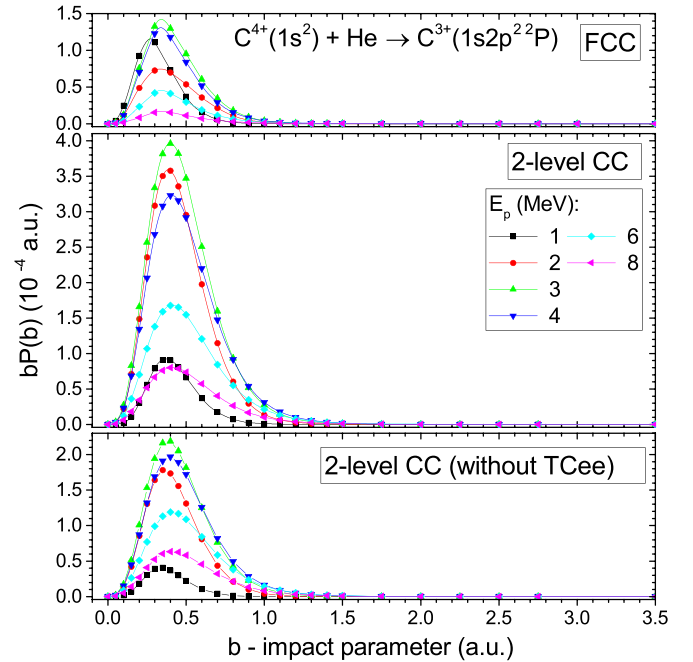


FIG. 7. Same as Fig. 6, but for the identically configured $1s2p^2 \ ^2P$ state. Note that the large- b dependence at $E_p = 6$ and 8 MeV in Fig. 6 (middle panel) is totally absent in the corresponding middle panel above, as expected by the inverse Auger description of this process (see text).

In Fig. 5 (top), the 2D cross sections are shown for the full and restricted 3eAOC calculations. As a first general observation, one can see that the cross sections from the FCC and the two-level CC calculations show similar structures, with two peaks. However, observed quantitative differences clearly demonstrate that even in this high energy regime, couplings to other states included in the FCC calculations, but removed in the two-level CC, are important. Only above 12 MeV do both calculations converge, as expected. In comparison, for the 2P cross sections, as shown in Fig. 5 (bottom), no high-energy peak is seen, in any of the 3eAOC calculations. In the next two sections we analyze in detail the two observed structures.

B. The high-energy peak and RTE

We first consider the 2D high-energy (~ 6 MeV) peak attributed to RTE (see Fig. 3). When the two-center bielectronic repulsion matrix elements are not taken into account, the resulting cross sections [green line in Fig. 5 (top)], do not show the high-energy peak, contrary to the FCC and two-level CC calculations. The origin of these differences is clearly elucidated when analyzing the 2D TE probabilities as a function of impact parameter b (Fig. 6): the large- b contribution present in the FCC and two-level CC calculations above 4 MeV, as seen in Fig. 6 (top and middle), is wiped out when the TCee interactions are removed [Fig. 6 (bottom)]. Additional evidence for the two-center (e-e) interactions character of the high-energy peak is provided by (i) the strong $M_L = 0$ contributions in this energy regime observed in the FCC calculations shown in Fig. 4, and (ii) the absence of the high energy TE peak in the case of the identically configured $1s2p^2$ 2P cross section, shown in Fig. 5 (bottom). Indeed, this state has an Auger decay rate about 10^4 smaller than the 2D [63] and therefore its production can be expected to be of negligible importance. This is clearly demonstrated by the IA RTE results shown in Fig. 5 (bottom). However, our FCC 2P calculation is seen [black line Fig. 5 (bottom)] to be only about a factor of 15 smaller than that for the 2D around the RTE maximum at 6 MeV. This surprisingly large difference between our FCC calculations and the IA RTE for the 2P cross sections can be traced to the fact that in ion-atom collisions in general, no selection rules apply during the excitation stage of the collision, while in the inverse Auger model of the IA RTE approximation, Auger selection rules are tacitly assumed in the production of the 2P and included in the expression for the $\sigma_{\text{RTE}}^{\text{IA}}$ cross section [see Ref. [9] Eqs. (9) and (10)]. This is further supported when analyzing the probabilities for the 2P state shown in Fig. 7: the FCC and both two-level calculations do not show any large- b tail as seen for the 2D , mainly due to the suppression of the two-center (e-e) interaction in this case. From these different results one can state that the high-energy 2D peak is therefore unambiguously mediated by the TCee interaction and consistent with the inverse Auger mechanism giving rise to its resonant character.

C. The low-energy peak and the NCTE mechanism

We next consider the low-energy (~ 2 MeV) peak for the 2D state, to date interpreted by a two-step mechanism [14,28].

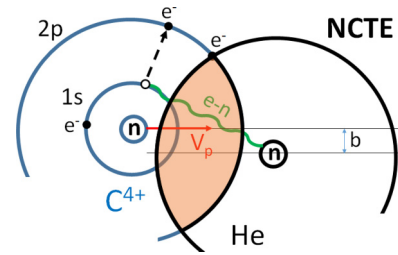


FIG. 8. As in Fig. 1, but for the process of nonresonant correlated transfer excitation (NCTE). Here the transfer occurs during the overlap (represented schematically by the orange area) of the electron clouds when the two partners are close by [$\langle 2p | 1s \rangle$ term in Eq. (12)] contributing primarily to the low-energy peak where transfer is strongest, while the projectile excitation is mediated by the (e-n) interaction [$\langle 2p | V^T | 1s \rangle$ term in Eq. (12)].

Since our two-level calculations still show this peak even though successive excitation and single electron capture (the main mechanism responsible for NTE, see Fig. 1) have been deliberately excluded in these calculations, its origin must necessarily arise from a *one-step* mechanism. Furthermore, additionally removing also the TCee interaction [green line in Fig. 5 (top)], the total cross sections still show the low-energy peak, albeit somewhat reduced in magnitude, indicating that the production of 2D in the two-level CC (blue line) is mediated by (e-e) and still to some effect by (e-n) interactions in this energy range. These unexpected results challenge our present understanding of transfer excitation at low collision energies. Moreover, looking into the b dependencies of Fig. 6, we note that the removal of the TCee interaction (bottom) leaves the shape of the reduced probability curves qualitatively unchanged in the low- b region. Thus, the low-energy peak observed in Fig. 5, arises primarily from this small impact parameter structure. Similar to the two-level CC results, the FCC results (top) also show the same unique low- b structure in the 1–3 MeV energy range, where the low-energy peak appears in the cross sections. These unexpected low-energy results point to the existence of a nonresonant but *correlated* (i.e., since must be single-step) transfer excitation (NCTE) mechanism. For higher E_p energies, the two well-separated $bP(b)$ structures in the two-level CC results (middle), are seen to merge in the FCC results (top), demonstrating the necessity for a coherent description of the two mechanisms.

We note that for the $1s2p^2$ 2P state a low-energy peak is also evident (see bottom panel of Fig. 5), even though the high-energy peak is absent. This is consistent with the proposed NCTE mechanism (see Fig. 8) for which an (e-n) interaction is responsible for the $1s \rightarrow 2p$ excitation of the projectile (similar for both identically configured states), while transfer is possible due to the overlap of the projectile $2p$ and target orbitals. In addition, as seen in Fig. 7, the impact parameter dependence of the $1s2p^2$ 2P state is also very similar to that for the 2D (Fig. 6), with the notable exception that the large- b dependence at $E_p = 6$ and 8 MeV is totally absent as expected by the much suppressed inverse Auger description of this process already discussed.

D. Further insights using the OBK model

The present results indicate that full close-coupling calculations are required to accurately describe transfer excitation. However, the complex coupling channel schemes involved make the extraction of underlying mechanisms and models from these calculations quite awkward. Nevertheless, it is very instructive to see a clear signature of both head-on (small b) and distant (large b) collision regimes in the semiclassical probability representation. An elucidating model may then be provided by applying to our process the Oppenheimer-Brinkman-Kramers (OBK) approximation in its prior form [57]. The perturbation in our three-electron approach can then be written as

$$W = V^T(r_i) + V^T(r_j) - \frac{Z_p}{r_k} + \frac{1}{r_{ik}} + \frac{1}{r_{jk}}, \quad (10)$$

where initially electrons i and j are bound to the projectile and electron k to the target. In Eq. (10), Z_p is the carbon nuclear charge and V^T is the model potential describing the interaction between an electron and He^+ [51]. The OBK time-integral

$$\left| -i \int_{-\infty}^{+\infty} dt \langle \Psi_f | W | \Psi_i \rangle e^{-i\Delta E_{if}t} \right|^2 \quad (11)$$

involves the coupling matrix element $W_{fi}(t) = \langle \Psi_f | W | \Psi_i \rangle$, where the initial $\text{C}^{4+}(1s^2) + \text{He}(1s)$ and final $\text{C}^{3+}(1s2p^2 \ ^2D)$ states can be approximately expressed in terms of Slater determinants $\Psi_i = |1s\bar{1}s\bar{1}s|$ and $\Psi_f = (|1s2p2p'| - |\bar{1}s2p2p'|)/\sqrt{2}$, respectively. Here the bar above the $n\ell$ orbitals stands, as usual, for spin-down electrons and the orbital $\bar{1}s$ is centered on He, while $1s$ and the two orthogonal (or identical) $2p, 2p'$ travelling orbitals are centered on the carbon. $\Delta E_{if} = E_i - E_f - V_p^2/2$ is the energy difference between the initial and final states, augmented by the kinetic part of the electron translation factor [57]. W_{fi} is then easily expressed as the sum of two terms

$$\sqrt{2}W_{fi} = \langle 2p|V^T|1s\rangle \langle 2p'|1s\rangle + \langle 2p2p'| \frac{1}{r_{ik}} |1s\bar{1}s\rangle. \quad (12)$$

The first term represents the $1s \rightarrow 2p$ excitation of the projectile by the target core (V^T), together with the transfer of the target electron to the projectile mediated by the two-center overlap, $\langle 2p'|1s\rangle$, when the two partners are close by. The second term $\langle 2p2p'| \frac{1}{r_{ik}} |1s\bar{1}s\rangle$ is a two-center bielectronic repulsion matrix element, the so-called TCee interaction. The expression in Eq. (12), though derived from a first-order treatment with known drawbacks [57], highlights the two mechanisms responsible for the two peaks shown in the cross sections. On the one hand, the second term is dominantly responsible for the high-energy peak due to RTE. On the other hand, the low-energy peak stems mainly from the first term and therefore corresponds to a nonresonant correlated transfer excitation (NCTE) mechanism (see Fig. 8). Here both transfer and excitation are induced simultaneously and of a different nature from the uncorrelated two-step mechanisms advocated in the past [14,28]. The relative magnitude of the two terms, as a function of the internuclear distance R and impact energy, is awkward to address since their actual values depend also on the mathematical expressions of the initial

and final states. Nevertheless, the Taylor series in $1/R$ of the Coulomb operators in $\langle 2p|V^T|1s\rangle$ and the two-center interelectronic Coulomb repulsion appearing in the TCee matrix element shows that to the nonvanishing first order, the two terms are close in magnitude (but of opposite sign), while to second order, $\langle 2p|V^T|1s\rangle$ is proportional to an electric quadrupole interaction, while TCee corresponds to an electric dipole interaction. Thus, at large impact parameters, the TCee term in Eq. (12) dominates for our considered final electronic configurations with two electrons in the $2p$ orbitals. This is in agreement with the impact parameter results shown in Fig. 6.

Finally, note that although interferences between all pathways leading to the same final state are inherently included in our close-coupling treatment, we do not see clear evidence of them in our cross sections, as advocated in previous investigations [5,16,25,28,30–32,34,36,64,65]. However, even in the much simpler OBK model giving rise to Eq. (12) and a simple expression for each TE mechanism, the W_{fi} matrix element must be integrated over time before its modulus is squared [see Eq. (11)]. Any discussion concerning the cross term of Eq. (12) as a signature of interference [5] is therefore not of a simple and direct matter. Our own quantitative description of TE requires a nonperturbative many-state approach, in which all couplings and pathways are coherently considered and accumulated during the collision. These then carry all possible interferences between the various mechanisms, but in a very complex form, not reducible to a simple cross term as given in Ref. [5], and therefore difficult to assess and unambiguously verify.

Further experimental results at low energies should be of interest to probe the mechanism presented in the previous section. However, such measurements in the energy range of 1–4 MeV would require almost pure $\text{C}^{4+}(1s^2)$ ion beams (to avoid additional TE from the metastable components [22,66], non-negligible at these much lower energies) and will be difficult to presently obtain at existing highly charged ion facilities (e.g., ECR sources) mostly due to the rather elevated, high-voltage (~ 0.25 –1 MV) platforms required.

V. SUMMARY AND CONCLUSION

We have presented results of a nonperturbative, multielectron treatment of transfer excitation in energetic collisions of He-like ground state ions with helium. All coupling schemes populating the same doubly excited state are included in one uniform and coherent treatment. We focus on the production of the $\text{C}^{3+}(1s2p^2 \ ^2D)$ states in collisions of $\text{C}^{4+}(1s^2)$ with helium, where our theoretical single differential cross sections show a distinctive two-peak structure as a function of the collision energy. We also present $\text{C}^{3+}(1s2p^2 \ ^2D)$ single differential cross sections based on high resolution Auger electron measurements. For the high-energy peak, there is excellent agreement between experiment and theory in the energy range where they overlap, i.e., at resonance (6 MeV) and beyond. Using simplifying two-level models, we have exposed the underlying mechanisms essentially responsible for these two peaks. The high-energy peak arises predominantly from the two-center electron-electron interaction in soft collisions, i.e., at large impact parameters, validating therefore our present understanding. However, the low-energy peak is found to

arise mainly from a one-step mechanism. It is mediated by a single electron-nucleus interaction responsible for excitation correlated to an electron transfer in head-on collisions, i.e., at small impact parameters, where the target and projectile electronic clouds largely overlap. Finally, concerning the interferences advocated in the past, our calculations inherently include them in our coherent treatment, but the total cross sections do not show any significant evidence of their presence.

Thus, even after almost 40 years since the introduction of the RTE and NTE mechanisms to explain transfer excitation, the presence of an additional one-step mechanism is revealed by a full quantum mechanical treatment, providing further insights into bielectronic processes in many-body quantum systems. To further deepen our knowledge of transfer excitation, we suggest two directions of great interest for the future: The study of other He-like ions, particularly in the low collision energy range, and investigations of differential cross

sections as a function of scattering angle, e.g., possibly using recoil ion momentum spectroscopy [67].

ACKNOWLEDGMENTS

We thank Nicolas Sisourat and Brett DePaola for valuable discussions. We also thank the staff of the “Demokritos” Tandem Accelerator Laboratory for their help with the measurements. We acknowledge support of this work by the project “Cluster of Accelerator Laboratories for Ion-Beam Research and Applications - CALIBRA” (MIS 5002799) which is implemented under the Action “Reinforcement of the Research and Innovation Infrastructure,” funded by the Operational Programme “Competitiveness, Entrepreneurship and Innovation” (NSRF 2014-2020) and co-financed by Greece and the European Union (European Regional Development Fund).

-
- [1] M. J. J. Vrakking and F. Lepine, Eds., *Attosecond Molecular Dynamics*, Theoretical and Computational Chemistry Series (The Royal Society of Chemistry, London, 2019), pp. 1–500.
- [2] Z. Tao, C. Chen, T. Szilvási, M. Keller, M. Mavrikakis, H. Kapteyn, and M. Murnane, Direct time-domain observation of attosecond final-state lifetimes in photoemission from solids, *Science* **353**, 62 (2016).
- [3] B. Vodungbo, B. Tudu, J. Perron, R. Delaunay, L. Müller, M. H. Berntsen, G. Grübel, G. Malinowski, C. Weier, J. Gautier, G. Lambert, P. Zeitoun, C. Gutt, E. Jal, A. H. Reid, P. W. Granitzka, N. Jaouen, G. L. Dakovski, S. Moeller, M. P. Minittie *et al.*, Indirect excitation of ultrafast demagnetization, *Sci. Rep.* **6**, 18970 (2016).
- [4] J. R. Sabin and E. J. Brändas, Eds., *Löwdin Volume*, Advances in Quantum Chemistry, Vol. 74 (Academic, New York, 2017), pp. 2–392.
- [5] J. M. Feagin, J. S. Briggs, and T. M. Reeves, Simultaneous charge transfer and excitation, *J. Phys. B* **17**, 1057 (1984).
- [6] J. A. Tanis, E. M. Bernstein, W. G. Graham, M. Clark, S. M. Shafroth, B. M. Johnson, K. W. Jones, and M. Meron, Resonant Behavior in the Projectile X-Ray Yield Associated with Electron Capture in S + Ar Collisions, *Phys. Rev. Lett.* **49**, 1325 (1982).
- [7] M. Clark, D. Brandt, J. K. Swenson, and S. M. Shafroth, Nonresonant Electron Transfer and Projectile K-Electron Excitation in Ion-Atom Collisions, *Phys. Rev. Lett.* **54**, 544 (1985).
- [8] L. S. Cederbaum, J. Zobeley, and F. Tarantelli, Giant Intermolecular Decay and Fragmentation of Clusters, *Phys. Rev. Lett.* **79**, 4778 (1997).
- [9] T. J. M. Zouros, Resonant transfer and excitation associated with Auger electron emission, in *Recombination of Atomic Ions*, edited by W. G. Graham, W. Fritsch, Y. Hahn, and J. Tanis, NATO Advanced Study Institute Series B: Physics, Vol. 296 (Plenum, New York, 1992), pp. 271–300.
- [10] T. Jahnke, U. Hergenbahn, B. Winter, R. Dörner, U. Fröhling, P. V. Demekhin, K. Gokhberg, L. S. Cederbaum, A. Ehresmann, A. Knie, and A. Dreuw, Interatomic and intermolecular Coulombic decay, *Chem. Rev.* **120**, 11295 (2020).
- [11] F. B. Rosmej, V. A. Astapenko, V. S. Lisitsa, and L. A. Vainshtein, Dielectronic recombination in non-LTE plasmas, *Matter Radiat. Extremes* **5**, 064201 (2020).
- [12] J. A. Tanis, E. M. Bernstein, M. W. Clark, W. G. Graham, R. H. McFarland, T. J. Morgan, B. M. Johnson, K. W. Jones, and M. Meron, Evidence for uncorrelated electron capture and K-shell excitation in S¹³⁺+He collisions, *Phys. Rev. A* **31**, 4040 (1985).
- [13] P. L. Pepmiller, R. Prichard, J. Newcomb, R. Dillingham, J. M. Hall, T. J. Gray, and M. Stöckli, A study of transfer excitation in F⁸⁺ + He, Ne and Ar collisions, *IEEE Trans. Nucl. Sci.* **30**, 1002 (1983).
- [14] D. Brandt, A simple classical model for the impact parameter dependence of electron capture, *Nucl. Instrum. Methods* **214**, 93 (1983).
- [15] J. A. Tanis, Resonant transfer excitation associated with single x-ray emission, in *Recombination of Atomic Ions*, edited by W. G. Graham, W. Fritsch, Y. Hahn, and J. Tanis, NATO Advanced Study Institute Series B: Physics, Vol. 296 (Plenum, New York, 1992), pp. 241–257.
- [16] A. Itoh, T. J. M. Zouros, D. Schneider, U. Stettner, W. Zeitz, and N. Stolterfoht, Transfer excitation in He⁺ + He collisions studied by zero-degree electron spectroscopy, *J. Phys. B* **18**, 4581 (1985).
- [17] J. K. Swenson, Y. Yamazaki, P. D. Miller, H. F. Krause, P. F. Dittner, P. L. Pepmiller, S. Datz, and N. Stolterfoht, Observation of Resonant Transfer and Excitation to Specific LS-Coupled states in O⁵⁺+He Collisions by High-Resolution, 0° Auger-Electron Spectroscopy, *Phys. Rev. Lett.* **57**, 3042 (1986).
- [18] T. J. M. Zouros, D. H. Lee, P. Richard, J. M. Sanders, J. L. Shinpaugh, S. L. Varghese, K. R. Karim, and C. P. Bhalla, State-selective observation of resonance transfer excitation (RTE) in collisions of F⁶⁺ with He and H₂ targets, *Phys. Rev. A* **40**, 6246 (1989).
- [19] T. J. M. Zouros, C. P. Bhalla, D. H. Lee, and P. Richard, Effects of alignment and interference in resonant transfer and excitation for F⁶⁺ and O⁵⁺ collisions with H₂ in 0° Auger measurements, *Phys. Rev. A* **42**, 678 (1990).
- [20] B. D. DePaola, R. Parameswaran, and W. J. Axmann, High-resolution state-selective study of transfer with

- excitation in the $F^{8+} + H_2$ system, *Phys. Rev. A* **41**, 6533 (1990).
- [21] B. DePaola, RTE studied in electron emission, *Nucl. Instrum. Methods Phys. Res., Sect. B* **56–57**, 154 (1991).
- [22] D. H. Lee, P. Richard, J. M. Sanders, T. J. M. Zouros, J. L. Shinpaugh, and S. L. Varghese, KLL resonant transfer and excitation to $F^{6+}(1s2l2l')$ intermediate states, *Phys. Rev. A* **44**, 1636 (1991).
- [23] R. Parameswaran, C. P. Bhalla, B. P. Walch, and B. D. DePaola, Resonant transfer and excitation in collisions of C^{5+} with H_2 and He targets, *Phys. Rev. A* **43**, 5929 (1991).
- [24] J. M. Anthony, S. M. Shafroth, M. Benhenni, E. N. Strait, T. J. M. Zouros, L. D. Hendrik, and D. M. Peterson, Production of doubly core-excited configurations in C^{4+} projectiles through resonant transfer excitation, *J. Phys. Colloques* **48**, C9-301 (1987).
- [25] M. Benhenni, S. M. Shafroth, J. K. Swenson, M. Schulz, J. P. Giese, H. Schöne, C. R. Vane, P. F. Dittner, and S. Datz, Angular Distribution of Auger Electrons Emitted through the Resonant Transfer and Excitation Process Following $O^{5+} + He$ Collisions, *Phys. Rev. Lett.* **65**, 1849 (1990).
- [26] D. Brandt, Resonant transfer and excitation in ion-atom collisions, *Phys. Rev. A* **27**, 1314 (1983).
- [27] E. P. Benis, T. J. M. Zouros, T. W. Gorczyca, A. D. González, and P. Richard, Elastic resonant and nonresonant differential scattering of quasifree electrons from $B^{4+}(1s)$ and $B^{3+}(1s^2)$ ions, *Phys. Rev. A* **69**, 052718 (2004); **73**, 029901(E) (2006).
- [28] W. Fritsch and C. D. Lin, Analysis of Electron Correlation in Simultaneous Electron Transfer and Excitation in Atomic Collisions, *Phys. Rev. Lett.* **61**, 690 (1988).
- [29] A. Jain, R. Shingal, and T. J. M. Zouros, State-selective non-resonant transfer excitation (NTE) in 50–500 keV $^3He^+ + H_2$ and He collisions, *Phys. Rev. A* **43**, 1621 (1991).
- [30] M. Benhenni, S. M. Shafroth, J. K. Swenson, M. Schulz, J. P. Giese, H. Schone, C. R. Vane, P. F. Dittner, and S. Datz, Evidence for interference between resonant and nonresonant transfer and excitation, in *Proceedings of the XVII ICPEAC held in Brisbane, Australia, 10-16 July 1991*, edited by W. R. McGillivray, I. E. McCarthy, and M. C. Standage (Adam Hilger, Bristol, England, 1992), pp. 693–698.
- [31] M. Benhenni, S. M. Shafroth, and J. K. Swenson, Alignment in fast ion-atom collisions, *Nucl. Instrum. Methods Phys. Res., Sect. B* **86**, 28 (1994).
- [32] M. Ourdane, H. Bachau, R. Gayet, and J. Hanssen, Transfer and excitation in high-energy $He^+ - He$ collisions: V. Electronic continuum influence on ejected electron distributions and TE cross sections, *J. Phys. B* **32**, 2041 (1999).
- [33] N. Stolterfoht, Dielectronic processes and electron correlation in energetic ion-atom collisions, *Nucl. Instrum. Methods Phys. Res., Sect. B* **53**, 477 (1991).
- [34] H. Bachau, R. Gayet, J. Hanssen, and A. Zerarka, Transfer and excitation in ion-atom collisions at high impact velocities: A unified continuum distorted wave treatment of resonant and non-resonant modes in four body approach: II. Application to the collisions $S^{15+}(1s) + H(1s)$, *J. Phys. B* **25**, 839 (1992).
- [35] R. Gayet, J. Hanssen, and L. Jacqui, Transfer and excitation in ion-atom collisions at high impact velocities: III. Application of the CDW-4B theory to an almost symmetrical system: $He^+ + He$, *J. Phys. B* **28**, 2193 (1995).
- [36] R. Gayet, J. Hanssen, L. Jacqui, and M. A. Ourdane, Transfer and excitation in ion-atom collisions at high impact velocities: IV. Application of the CDW-4B theory to an almost symmetrical system: $He^+ + H$, *J. Phys. B* **30**, 2209 (1997).
- [37] T. J. M. Zouros, D. Schneider, and N. Stolterfoht, State-selective observation of resonant and non-resonant transfer excitation in 50–500 keV $^3He^+ + H_2$ collisions, *J. Phys. B* **21**, L671 (1988).
- [38] T. J. M. Zouros and D. H. Lee, Zero degree Auger electron spectroscopy of projectile ions, in *Accelerator-Based Atomic Physics: Techniques and Applications*, edited by S. M. Shafroth and J. C. Austin (AIP, Woodbury, NY, 1997), Chap. 13, pp. 426–479.
- [39] J. W. Gao, Y. Wu, J. G. Wang, A. Dubois, and N. Sisourat, Double Electron Capture in $H^+ + H^-$ Collisions, *Phys. Rev. Lett.* **122**, 093402 (2019).
- [40] I. Madesis, A. Laoutaris, S. Nanos, S. Passalidis, A. Dubois, T. J. M. Zouros, and E. P. Benis, State-resolved differential cross sections of single electron capture in swift collisions of $C^{4+}(1s2s^3S)$ ions with gas targets, *Phys. Rev. A* **105**, 062810 (2022).
- [41] S. Harissopoulos, M. Andrianis, M. Axiotis, A. Lagoyannis, A. G. Karydas, Z. Kotsina, A. Laoutaris, G. Apostolopoulos, A. Theodorou, T. J. M. Zouros, I. Madesis, and E. P. Benis, The Tandem Accelerator Laboratory of NCSR Demokritos: Current status and perspectives, *Eur. Phys. J. Plus* **136**, 617 (2021).
- [42] I. Madesis, A. Laoutaris, T. J. M. Zouros, S. Nanos, and E. P. Benis, Projectile electron spectroscopy and new answers to old questions: Latest results at the new atomic physics beamline in Demokritos, Athens, in *State-of-the-Art Reviews on Energetic Ion-Atom and Ion-Molecule Collisions*, Interdisciplinary Research on Particle Collisions and Quantitative Spectroscopy, Vol. 2, edited by D. Belkić, I. Bray, and A. Kadyrov (World Scientific, Singapore, 2019), Chap. 1, pp. 1–31.
- [43] D. H. Lee, P. Richard, T. J. M. Zouros, J. M. Sanders, J. L. Shinpaugh, and H. Hidmi, Binary encounter electrons observed at zero degrees in collisions of 1–2 MeV/amu H^+ , C^{6+} , N^{7+} , O^{8+} and F^{9+} , *Phys. Rev. A* **41**, 4816 (1990).
- [44] H. T. Schmidt, P. Forck, M. Grieser, D. Habs, J. Kenntner, G. Miersch, R. Repnow, U. Schramm, T. Schüssler, D. Schwalm, and A. Wolf, High-Precision Measurement of the Magnetic-Dipole Decay Rate of Metastable Heliumlike Carbon Ions in a Storage Ring, *Phys. Rev. Lett.* **72**, 1616 (1994).
- [45] E. P. Benis, I. Madesis, A. Laoutaris, S. Nanos, and T. J. M. Zouros, Mixed-state ionic beams: An effective tool for collision dynamics investigations, *Atoms* **6**, 66 (2018).
- [46] E. P. Benis and T. J. M. Zouros, Determination of the $1s2\ell 2\ell'$ state production ratios $^4P^o / ^2P$, $^2D / ^2P$ and $^2P_+ / ^2P_-$ from fast ($1s^2$, $1s2s^3S$) mixed-state He-like ion beams in collisions with H_2 targets, *J. Phys. B* **49**, 235202 (2016).
- [47] M. Zamkov, H. Aliabadi, E. P. Benis, P. Richard, H. Tawara, and T. J. M. Zouros, Energy dependence of the metastable fraction in $B^{3+}(1s^2\ ^1S, 1s2s\ ^3S)$ beams produced in collisions with thin-foil and gas targets, *Phys. Rev. A* **64**, 052702 (2001).
- [48] M. Zamkov, E. P. Benis, P. Richard, and T. J. M. Zouros, Fraction of metastable $1s2s\ ^3S$ ions in fast He-like beams ($Z = 5–9$) produced in collisions with carbon foils, *Phys. Rev. A* **65**, 062706 (2002).

- [49] E. P. Benis, M. Zamkov, P. Richard, and T. J. M. Zouros, Technique for the determination of the $1s2s\ ^3S$ metastable fraction in two-electron ion beams, *Phys. Rev. A* **65**, 064701 (2002).
- [50] E. P. Benis, M. Zamkov, P. Richard, and T. J. M. Zouros, Comparison of two experimental techniques for the determination of the $1s2s\ ^3S$ metastable beam fraction in energetic B^{3+} ions, *Nucl. Instrum. Methods Phys. Res., Sect. B* **205**, 517 (2003).
- [51] I. Madesis, A. Laoutaris, T. J. M. Zouros, E. P. Benis, J. W. Gao, and A. Dubois, Pauli Shielding and Breakdown of Spin Statistics in Multielectron Multi-Open-Shell Dynamical Atomic Systems, *Phys. Rev. Lett.* **124**, 113401 (2020), and Supplemental Material.
- [52] A. Laoutaris, S. Nanos, I. Madesis, A. Biniskos, E.P. Benis, S. Passalidis, A. Dubois, and T. J. M. Zouros, Production of $2s2p\ ^1,^3P$ states by $1s \rightarrow 2p$ excitation of He-like carbon and oxygen ions in 0.5–1.5 MeV/u collisions with He (unpublished).
- [53] I. Madesis, Investigation of electron capture in swift $C^{4+}(1s2s\ ^3S)$ collisions with gas targets using a zero-degree Auger projectile spectroscopy apparatus built with the L45 beam line at the “Demokritos” 5.5 MV tandem accelerator, Ph.D. thesis, University of Crete, Department of Physics, Heraklion, Greece, 2021.
- [54] N. Sisourat, I. Pilskog, and A. Dubois, Non perturbative treatment of multielectron processes in ion-molecule scattering: Application to He^{2+} - H_2 collisions, *Phys. Rev. A* **84**, 052722 (2011).
- [55] J. W. Gao, Y. Wu, J. G. Wang, N. Sisourat, and A. Dubois, State-selective electron transfer in He^+ +He collisions at intermediate energies, *Phys. Rev. A* **97**, 052709 (2018).
- [56] J. W. Gao, T. Miteva, Y. Wu, J. G. Wang, A. Dubois, and N. Sisourat, Single- and double-ionization processes using Gaussian-type orbitals: Benchmark on antiproton-helium collisions in the keV-energy range, *Phys. Rev. A* **103**, L030803 (2021).
- [57] M. R. C. McDowell and J. P. Coleman, *Introduction to the Theory of Ion-Atom Collisions* (North-Holland, New York, 1970).
- [58] W. Fritsch and C. D. Lin, The semiclassical close-coupling description of atomic collisions: Recent developments and results, *Phys. Rep.* **202**, 1 (1991).
- [59] W. Mehlhorn and K. Taulbjerg, Angular distribution of electrons from autoionising states with unresolved fine structure, *J. Phys. B* **13**, 445 (1980).
- [60] F. F. Goryaev, L. A. Vainshtein, and A. M. Urnov, Atomic data for doubly-excited states $2lnl'$ of He-like ions and $1s2lnl'$ of Li-like ions with $Z = 6$ –36 and $n = 2, 3$, *At. Data Nucl. Data Tables* **113**, 117 (2017).
- [61] R. A. Holt, M. H. Prior, K. L. Randall, R. Hutton, J. McDonald, and D. Schneider, Magnetic substates populated by double-electron capture, *Phys. Rev. A* **43**, 607 (1991).
- [62] N. R. Badnell, Auger emission following resonant transfer excitation in collisions of F^{8+} with H_2 , *Phys. Rev. A* **41**, 3555 (1990).
- [63] The two identically configured $1s2p^2\ ^2D$ and $1s2p^2\ ^2P$ states are very similar in that they both require the same net $1s \rightarrow 2p$ excitation and $2p$ transfer to be produced by TE. However, due to parity selection rules, the $1s2p^2\ ^2P$ state cannot autoionize within the LS coupling scheme. Its Auger energy is $\varepsilon'_A = 242.94$ eV, while its Auger rate and yield are particularly small at $A_a = 6.7 \times 10^9\ s^{-1}$ and $\bar{\xi} = 0.0110$, respectively [68], making it practically undetectable by Auger spectroscopy. In comparison, the $1s2p^2\ ^2D$ state’s Auger rate, energy and yield are $A_a = 9.316 \times 10^{13}\ s^{-1}$, $\varepsilon'_A = 242.1$ eV, and $\bar{\xi} = 0.9985$, respectively [68]. The $1s2p^2\ ^2P$ state can decay radiatively [69] and also by the more rare process of radiative autoionization [70,71].
- [64] R. Gayet and J. Hanssen, Transfer and excitation in ion-atom collisions at high impact velocities: A unified continuum distorted wave treatment of resonant and non-resonant modes in four body approach: I. Theory, *J. Phys. B* **25**, 825 (1992).
- [65] R. Gayet, J. Hanssen, and L. Jacqui, Corrigenda—Transfer and excitation in ion-atom collisions at high impact velocities: III. Application of the CDW-4B theory to an almost symmetrical system: $He^+ + He$, *J. Phys. B* **30**, 1619 (1997).
- [66] D. H. Lee, P. Richard, J. M. Sanders, T. J. M. Zouros, J. L. Shinpaugh, and S. L. Varghese, Electron capture and excitation studied by state-resolved KLL Auger measurement in 0.25–2 MeV/u $F^{7+}(1s^2\ ^1S, 1s2s\ ^3S) + H_2/He$ collisions, *Nucl. Instrum. Methods Phys. Res., Sect. B* **56–57**, 99 (1991).
- [67] R. Dörner, V. Mergel, O. Jagutzki, L. Spielberger, J. Ullrich, R. Moshammer, and H. Schmidt-Böcking, Cold target recoil ion momentum spectroscopy: A “momentum microscope” to view atomic collision dynamics, *Phys. Rep.* **330**, 95 (2000).
- [68] M. H. Chen, Dielectronic satellite spectra for He-like ions, *At. Data Nucl. Data Tables* **34**, 301 (1986).
- [69] J. L. Fox and A. Dalgarno, Radiative transition probabilities of the $1s2p^2\ ^2P$ and $1s2p^2\ ^2D$ states of the lithium isoelectronic sequence, *Phys. Rev. A* **16**, 283 (1977).
- [70] C. A. Nicolaidis and D. R. Beck, Comment on the lifetime of the Li $1s2p^2\ ^2P$ state: How probable is radiative autoionization?, *Phys. Rev. A* **17**, 2116 (1978).
- [71] T. Åberg and J. Utriainen, Evidence for a “Radiative Auger Effect” in X-Ray Photon Emission, *Phys. Rev. Lett.* **22**, 1346 (1969).